HHS Public Access

Author manuscript

Biotechnol Bioeng. Author manuscript; available in PMC 2015 June 18.

Published in final edited form as:

Biotechnol Bioeng. 2014 November ; 111(11): 2326–2337. doi:10.1002/bit.25291.

Effects of shear stress pattern and magnitude on mesenchymal transformation and invasion of aortic valve endothelial cells

Gretchen J. Mahler[a,b], **Christopher M. Frendl**[a], **Qingfeng Cao**[c], and **Jonathan T. Butcher**[a,*]

[a]Department of Biomedical Engineering, Cornell University, Ithaca, NY, USA

[c]Department of Mechanical Engineering, Binghamton University, Binghamton, NY, USA

Abstract

Understanding the role of mechanical forces on cell behavior is critical for tissue engineering, regenerative medicine, and disease initiation studies. Current hemodynamic bioreactors are largely limited to 2D substrates or the application of general flow conditions at a tissue level, which eliminates the investigation of some essential physiological and pathological responses. One example is the mesenchymal transformation of endothelial cells in response to shear stress. Endothelial to mesenchymal transformation (EndMT) is a valve morphogenic mechanism associated with aortic valve disease initiation. The aortic valve experiences oscillatory shear on the disease-susceptible fibrosa, and the role of hemodynamics on adult EndMT is unknown. The goal of this work was to develop and characterize a microfluidic bioreactor that applies physiologically relevant laminar or oscillatory shear stresses to endothelial cells and permits the quantitative analysis of 3D cell-extracellular matrix (ECM) interactions. In this study, porcine aortic valve endothelial cells were seeded onto 3D collagen I gels and exposed to different magnitudes of steady or oscillatory shear stress for 48 hours. Cells elongated and aligned perpendicular to laminar, but not oscillatory shear. Low steady shear stress (2 dyne/cm^2) and oscillatory shear stress upregulated EndMT- (ACTA2, Snail, TGFB1) and inflammation- (ICAM1, NFKB1) related gene expression, EndMT-related (αSMA) protein expression, and matrix invasion when compared with static controls or cells exposed to high steady shear (10 and 20 dyne/cm^2). Our system enables direct testing of the role of shear stress on endothelial cell mesenchymal transformation in a dynamic, 3D environment and shows that hemodynamics regulate EndMT in adult valve endothelial cells.

Keywords

3D culture; side specific; inflammation; endothelial to mesenchymal transformation

Introduction

The aortic valve ensures the unidirectional flow of oxygenated blood to the cardiovascular system. The aortic valve leaflets open and close 30–40 million times per year, subjecting these thin and flexible cusps to extremely demanding tissue strains and hemodynamic

*Fax: 1-607-255-7330; Tel: 1-607-255-3575; jtb47@cornell.edu.

[b]Current address: Department of Bioengineering, Binghamton University, Binghamton, NY, USA

stresses (Thubrikar et al. 1990). Alterations from normal valve homeostasis arise from genetic and microenvironmental (mechanical) sources, which can lead to congenital and/or premature structural degeneration (Butcher et al. 2011). The huge number of stress cycles applied to the valve can be endured only by continuous remodeling of the valve matrix by resident cells (Schneider and Deck 1981). One potential mechanism of valve repair and potentially early valve disease is through endothelial to mesenchymal transformation (EndMT), the initiating event of valvulogenesis (Markwald et al. 1977; Markwald et al. 1975). Soluble factors (TGFβ-1, TNFα) (Mahler et al. 2013; Paranya et al. 2001) and pathological cyclic strain (Balachandran et al. 2011) have individually been shown to induce this key cell transformation in adult valve endothelial cells.

In the developing embryo, endocardial cells lining the early U-shaped heart transform to an embryonic fibroblast phenotype and invade and populate the endocardial cushions that will eventually develop into mature atrioventricular and semilunar valves (Markwald et al. 1977). The process of EndMT begins when a subset of endothelial cells lose cell-cell contacts and separate from the monolayer. These cells then lose endothelial markers such as CD31/PECAM-1, gain mesenchymal markers like alpha smooth muscle actin (αSMA), and invade and migrate into the underlying interstitial space (Nakajima et al. 1997). The role of EndMT in adult valve physiology is unknown, but it has been suggested to be a natural cell replenishment mechanism or a mechanism of disease (Mahler et al. 2013; Paranya et al. 2001). It is therefore important to understand the mechanism of EndMT, of which hemodynamics is an understudied component.

The physiological role of valvular endothelial cells includes controlling the coagulation response, regulation of underlying interstitial cells, and the transmittance or clearance of compounds from the blood (Butcher and Nerem 2007). Valve pathology has been shown to originate from systemic endothelial dysfunction and this could be due to the ability of endothelial cells to sense and respond to mechanical and biochemical signals (Poggianti et al. 2003). Fluid flow profiles are very different on each side of the valve, and fluid shear stress can modulate valve endothelial cell behavior (Butcher et al. 2004). The inflow (ventricularis) surface is exposed to a rapid, pulsatile, unidirectional shear stress; while the outflow (arterial or fibrosa) surface experiences a much lower velocity, oscillatory shear stress (Kilner et al. 2000). *In vivo* observations of valve disease have shown that inflammatory and calcific degeneration initiates on the oscillatory shear-exposed, fibrosa side of the valve (Mohler 2000; Mohler 2004; Mohler et al. 2001). Oscillatory shear may, therefore, induce valve pathology.

Fluid shear stress can modulate endothelial cell behavior and is relevant to normal valvular physiology and the pathogenesis of valvular disease (Butcher and Nerem 2006; Butcher et al. 2004; Butcher et al. 2006). Shear stress values on the aortic valve surface are difficult to quantify due to the rapid and constant motion of the leaflets, but shear stresses ranging from 30 to 1,500 dyne/cm^2 have been reported, with an average shear stress rate of approximately 20 dyne/cm^2 over the valve ventricularis across the cardiac cycle (Nandy and Tarbell 1987; Weston et al. 1999). More recent simulations by Yap et al. have shown that at a heart rate of 70 beats/min and a 73 mL stroke volume, the shear over the valve fibrosa peaks at 21.3 dyne/cm^2 during mid-systole and gradually decreased to zero over the diastolic duration

(Yap et al. 2012a). Simulations of the aortic valve ventricularis by the same group show a peak systolic shear stress of at 64–71 dyne/cm^2 (Yap et al. 2012b). For adult valve endothelial cell experiments with PAVEC, the cells were exposed to 2, 10, or 20 dyne/cm^2 steady shear stress or ±2, 10, or 20 dyne cm^2 oscillatory shear stress, which falls within the range of physiological values and are reasonable time-averaged approximations of the flow environment.

Previous work has shown that shear induces EndMT in embryonic endothelial cells (Egorova et al. 2011; ten Dijke et al. 2012), although no studies have yet been performed to determine how different shear stress profiles modulate adult EndMT. Studying EndMT under physiological conditions is critical for clarifying its role in valve disease, but the complexity of the *in vivo* environment makes identifying the specific effects of mechanical stimuli challenging. The aortic heart valve microenvironment includes soluble growth factors, cell-cell and cell-ECM interactions, and physical forces. The role and integration of these complex elements, however, remains poorly understood.

The goal of this work is to develop a parallel plate bioreactor with 3D culture that can recreate critical components of the dynamic aortic valve environment, and to use this bioreactor to determine the role of differing shear stress profiles on EndMT in adult valve endothelial cells. Our shear stress bioreactor allows us to expose valve endothelial cells seeded on a physiologically realistic 3D matrix to varying steady or oscillatory shear stresses, with multiple shear stresses in the same experimental run. We are also able to add the 3D collagen I matrix and seed cells before the device is sealed and, although co-cultures were beyond the scope of these experiments, in future work we will be able to co-culture cells in 3D that have direct contact as opposed to being separated by a membrane. These are improvements over previous 3D culture and oscillatory shear microfluidic bioreactors (Chen et al. 2013a; Chen et al. 2013b; Hsu et al. 2013; Shao et al. 2009; Vickerman et al. 2008). The flow profile within the bioreactor was characterized both computationally and experimentally. Endothelial cell alignment, invasion, and EndMT-related gene and protein expression was evaluated following exposure to varying rates of steady and oscillatory shear and compared with static cultures.

Materials and Methods

Bioreactor design and fabrication

An exploded diagram of the bioreactor is shown in Figure 1A. The bioreactor consists of three parallel chambers, each 21 mm wide, 65 mm long, and 0.4 mm high. These chambers were created with three machined, 114 mm × 95 mm polycarbonate sheets (McMaster-Carr, Santa Fe Springs, CA). The bottom sheet is composed of 6.35 mm (1/4”) polycarbonate that contains nine 6.5 mm diameter, 3 mm deep holes. This design allows for three replicates at each shear stress. These holes were drilled so they would be located in the center of each chamber, be 11.375 mm from the chamber inlet, and be 11.375 mm apart. The middle sheet is made up of 0.4 mm (0.016”) polycarbonate that was machined with three rectangular holes that are 65 mm long, 21 mm wide, 8 mm from the sides of the sheet and 8 mm apart, and 24.5 mm from both ends of the sheet. The top sheet is composed of 12.7 mm (1/2”) polycarbonate with holes at the inlet and outlet (5 mm in from the edge of the sheet and 45

mm in from the side of the sheet) threaded to fit kynar PVDF female luers with a 5/16" hex to 1/4–28 UNF thread (#SFTLL-J1A, Value Plastics, Inc., Fort Collins, Colorado). On the top face of the top sheet, Kynar PVDF male luers with an integral lock ring to 200 series barb for 1/8" (3.2 mm) internal diameter tubing (#MTLL230-J1A, Value Plastics, Inc.) were connected to the female luers. On the bottom side of the top sheet were 0.4 mm deep machined channels that led from the inlet and outlet to the chambers. The channels are 0.42 mm wide (leads to side, low shear chamber), 0.91 mm wide (leads to middle, high shear chamber), and 1.2 mm wide (leads to side, medium shear chamber). The chambers and channels were designed so that the pressure drop was the same for each, allowing for a passive fluid flow split at the bioreactor inlet. All parts except for the middle 0.4 sheet are autoclavable; the 0.4 mm sheet was soaked in 70% ethanol for 15 minutes for sterilization.

The bioreactor was designed to provide physiologically relevant levels of steady or oscillatory shear stress over the surface of endothelial cells growing on top of a 3D ECM matrix. Assuming fully developed, incompressible, laminar flow in the rectangular-shaped channels of the bioreactor, shear stress is a function of the channel geometry, flow rate, and fluid viscosity according to Equation (1):

$$\tau_w = 6Q\mu/h^2w \quad (1)$$

Where τ_w is the shear stress at the top and bottom surfaces of the chambers, μ is the fluid viscosity, Q is the volumetric flow rate, h is the height of the chamber, and w is the width of the chamber. Viscosity was assumed to be 3.3×10^{-3} Pa•s (Sun and Yokota 2001) and density to be 1.1×10^{3} kg/m^3. For rectangular microchannels, this numerical approximation agrees well with three-dimensional computation fluid dynamics simulations (Lu et al. 2004).

Bioreactor assembly and operation

After the 3D collagen constructs were added to the bottom sheet and cells were seeded onto those constructs and allowed to attach for four hours (described below), the device was assembled. The three polycarbonate sheets were held together with 22 1” length, 4–40 thread, 18/8 stainless steel screws. Silicone tubing (1/4” OD, 1/8” ID, Cole-Parmer, Vernon Hills, IL) was used to connect the bioreactor inlet and outlet to all other components. For steady shear experiments, flow was generated with a Masterflex L/S Brushless variable-speed digital drive; Masterflex L/S 8-channel, 4-roller cartridge pump head; and Masterflex L/S large cartridges (Cole-Parmer). A polyethylene pulse dampener (Cole-Parmer) filled with 25 mL of medium was placed in between the peristaltic pump and bioreactor in the circuit in order to eliminate pulsation in output flow. The steady shear circuit was completed with a 250 mL polycarbonate reservoir bottle with a filling/venting cap for 1/4" tubing (Nalge Nunc International, Rochester, NY) filled with 100 mL culture medium. The peristaltic pump was operated at flowrate of 24.3 mL/min during 48 hour experiments and the entire assembly was kept at 37°C and 5% CO_2 within an incubator.

For oscillatory shear experiments flow was generated with an Aladdin-6000 syringe pump (World Precision Instruments, Sarasota, FL). A square wave ±24.3 mL/min flow pattern at 1 Hz was used, in which the flow was fully forward at 2, 10 or 20 dynes/cm^2 for one-half of the cycle and fully reversed at −2, 10 or 20 dynes/cm^2 for the remainder of the cycle. The

oscillatory shear set-up was composed of the syringe pump with a 60 mL syringe (BD Biosciences, San Jose, CA) filled with 50 mL culture medium, the bioreactor, and a 250 mL polycarbonate reservoir bottle with a filling/venting cap for 1/4" tubing (Nalge Nunc International) filled with 75 mL culture medium. The entire assembly was kept at 37°C and 5% CO_2 within an incubator for the 48 hour experiments. The bioreactor set-up for steady and oscillatory shear experiments is shown in Figure 1B–D.

Bioreactor characterization

ANSYS FLUENT v.14.5 was used to simulate the flow fields in the microfluidic chambers. These chamber models were developed with identical geometry and dimensions except for the inlet width. The inlet was maintained as the sole source of flow initiation in the model with identical dimensions to the outlet, which acted as the sole source of exit for flow.

Flow through the bioreactor was characterized experimentally for the steady and oscillatory shear flows in the low (2 dyne/cm^2), middle (10 dyne/cm^2), and high (20 dyne/cm^2) shear stress chambers. First, the residence time was measured by filling the holes in the bottom sheet with 1% agarose and timing the movement of the air-water interface as the chambers filled. To measure the linear velocity over the samples and verify that the collagen gels were flush with the polycarbonate sheet, 10 μm, polystyrene, yellow-green fluorescent microspheres (Polysciences, Inc., Warrington, PA) were added to PBS and flowed through the low, middle, and high shear channels under a total flowrate of 24.3 ml/min for steady shear conditions and ±24.3 ml/min at 1 Hz for oscillatory conditions. The bead flow in the channels was captured using a Nikon SMZ1000 stereomicroscope and a Sony DXC-390 camera. The digital recording program used was Streampix III (NorPix, Inc., Montreal, Quebec, Canada) with a pixeLINK video converter (Ottawa, Ontario, Canada). The steady shear files were processed using VirtualDub 1.9.11 and bead velocity was measured using Image J and the Manual Tracking plugin (Schneider et al. 2012).

Three dimensional collagen constructs

Three dimensional collagen gels at a concentration of 1.5 mg/mL collagen were made by combining ice-cold 3X Dulbecco's Modified Eagle's Medium (DMEM, Life Technologies, Grand Island, NY), 10% Fetal Bovine Serum (FBS, Life Technologies), sterile 18 MΩ water, 0.1 M NaOH, and rat tail collagen I (BD Biosciences). Bioreactor wells and static control wells (4 well tissue culture plates, 1.9 cm^2 growth area; Nalge Nunc International) were first coated with Cell-TAK tissue adhesive (BD Biosciences) by pipetting Cell-Tak diluted in PBS (50 μg/mL concentration) into each well. The solution was allowed to incubate at room temperature for 20 minutes and then removed. An aliquot of the collagen solution was subsequently pipetted into each bioreactor well or static well and allowed to gel for at least 1 hour at 37°C and 5% CO_2.

Porcine aortic valve endothelial cell isolation and culture

Porcine aortic valve endothelial cells were isolated and pooled from both sides of the valve using the method described by Butcher et al. and Gould and Butcher (Butcher et al. 2004; Gould and Butcher 2010). Porcine heart valves were kindly donated by Shirk Meats of Dundee, NY. Porcine aortic valve endothelial cells (PAVEC) were grown in flasks coated

with 50 μg/mL rat tail collagen I. Cells were cultured at 37°C and 5% CO_2 in DMEM supplemented with 10% FBS, 1% penicillin-streptomycin (Life Technologies), and 50 U/mL heparin (Sigma-Aldrich, St. Louis, MO). Culture medium was changed every 48 hours and cells were passaged with 0.05% Trypsin-EDTA (Life Technologies) at a 1:3 ratio at confluence. Endothelial culture purity was confirmed at passage 3 at the most conservative level via real-time PCR for ACTA2 (not expressed in valve endothelial cells but expressed in valve interstitial cells and in cells undergoing EndMT). Cultures with undetectable expression (cycle threshold > 37 cycles) were used in subsequent experiments.

For experiments, cells were seeded at a density of 50,000 cells/cm^2 at passage 5 on the surface of the collagen gels. After 4 hours, the bioreactor was assembled and sealed, DMEM culture medium was added to the liquid reservoir, and the cells were sheared at 2, 10, or 20 dynes/cm^2 for 48 hours. Static controls were seeded into well plates and were not exposed to shear flow. At the 48 hour time point the bioreactor was disassembled, gels were removed from the wells, and cells were immediately fixed for immunofluorescence in 4% paraformaldehyde or processed for RNA isolation.

Cell invasion

The cell invasion assay has been described in detail previously (Mahler et al. 2013). Briefly, adult valve endothelial cells were seeded onto the 3D collagen gel. After 48 hours in static or dynamic conditions, invaded, mesenchymally transformed cells were quantified using a 10X objective and an inverted microscope. First, the microscope was focused on the endothelial layer on the surface of the gel. Next the microscope was focused 60 μm down into the gel, and the number of in-focus invaded cells was quantified. This process was repeated for four fields in the center of the gel, resulting in 0.125 cm^2 of the 0.33 cm^2 growth area being analyzed.

Immunohistochemistry

Fixed samples on collagen gels were washed for 15 minutes on a rocker 3 times with PBS, permeabilized with 0.2% Triton-X 100 (VWR International, West Chester, PA) for 10 minutes, and washed another 3 times with PBS. Samples were then incubated overnight at 4°C in a 1% BSA (Rockland Immunochemicals, Inc., Gilbertsville, PA) blocking solution. For F-actin staining, gels were next exposed to 0.5 U phalloidin (Alexa Fluor® 488 Phalloidin, Invitrogen) in PBS for 30 minutes at room temperature. Phalloidin had previously been reconstituted in methanol per the manufacturer's instructions. For PECAM-1 and αSMA staining, gels were incubated overnight at 4°C with mouse anti-porcine PECAM-1 1:100 in PBS (AbD Serotech, Raleigh, NC) and rabbit anti-human αSMA 1:100 in PBS (Spring Bioscience, Pleasanton, CA). After 3 washes for 15 minutes with PBS, samples were then exposed to Alexa Fluor® 488 or 568 conjugated (Invitrogen), species-specific secondary antibodies at 1:100 in 1% BSA in PBS for 2 hours at room temperature. Three more washes with PBS for 15 minutes were followed by incubation with DRAQ5 far red nuclear stain (Enzo Life Sciences AG, Lausen, Switzerland) at 1:1000 in PBS. Samples were washed once more with 18 MΩ water and stored in 18 MΩ water at 4°C. Images were taken with a Leica TCS SP2 (Exton, PA) laser scanning confocal microscope. αSMA protein expression and total number of cells per image was quantified with ImageJ

software. Green (αSMA) channels from ten representative confocal images were each thresholded identically, and the thresholded stained area was quantified.

Morphological analysis

Ten representative confocal images were taken of static and sheared cells on 3D collagen I gels that were fixed and stained with phalloidin. The gels exposed to shear stress were aligned so that the image horizontal corresponded to the direction of flow. ImageJ was used to overlay polygons delineating cell areas according to F-actin filaments. The angle between the horizontal (flow direction) and the majority of F-actin filaments was also determined. Two indices of cell alignment were used: cell shape index (SI) and orientation angle (OA). SI is a non-dimensional parameter that quantifies cell elongation on a scale of 0 to 1, with 0 denoting a straight line, and 1 a perfect circle. It is represented by Equation (2):

$$\mathrm{SI}=4\pi \mathrm{A}/\mathrm{P}^2 \quad (2)$$

Where A is the cell area and P is the cell perimeter. Orientation angle was the deviation of the major actin filament axis from the slide horizontal, which was parallel to the flow direction. The shape index and cell orientation angle were determined for at least 50 cells.

Gene expression analysis

Total RNA was extracted from cells on 3D collagen gels using a Norgen total RNA purification kit (Norgen Biotek Corp., Thorold, Ontario, Canada) and RNA was reverse transcribed to cDNA using the SuperScript III RT-PCR kit with oligo(dT) primer (Invitrogen). The three gels from each shear stress channel were pooled for RNA isolations. RT-PCR was performed on all samples using SYBR Green PCR master mix (Applied Biosystems, Foster City, CA) and a MiniOpticon Real-Time PCR Detection System (Biorad, Hercules, CA). Primer sequences have previously been published (Mahler et al. 2013).

Statistical analysis

Results are expressed as mean ± standard error. Data was analyzed with GraphPad Prism version 5.00 for Windows (GraphPad Software, San Diego, CA). Results were analyzed by one-way ANOVA followed by Tukey's post-test. Differences between means were considered significant at $p < 0.05$.

Results

The flow fields in the three microfluidic chambers under steady shear stress were simulated by ANSYS FLUENT v.14.5. The varied flow rates initiated different streamline distributions and shear stress levels around the central region at the bottom wall of the three chambers. Figures 2A–C show the fluid streamlines for the three chambers and the corresponding wall shear stress at nine different sample points within each chambers. This simulation validates our hypothesis of uniform shear being experienced across the central region of the chamber bottom wall. This modeling also confirms our theoretical shear ranges, which were calculated based on Equation (1). Table I compares the calculated bioreactor chamber residence times and linear velocity with the experimentally measured

residence times and bead linear velocity. These results show that the experimentally measured residence time and linear velocity is within ~85% of the calculated values. The bead flow videos (see Supplemental Information) also show that the collagen gels were flush with the bottom polycarbonate sheet, as bead flow was not disturbed when passing over the gel when compared with flow over the polycarbonate to the sides of the gel.

Cell phenotype analysis following 48 hours of static culture or exposure to 2, 10, or 20 dyne/cm^2 steady or oscillatory shear is shown in Figures 3, 4 and 5. Paracrine effects of upstream cells on downstream cells are a possibility, however the relatively large volume of culture medium (125 mL) and the relatively small number of cells (2.97 cm^2 total growth area) make paracrine signaling unlikely. There were no differences found in alignment or invasion in downstream wells when compared with upstream wells. Both 2 dyne/cm^2 (14±3 invaded cells/10X field, $p < 0.01$) and 10 dyne/cm^2 (13±2 invaded cells/10X field, $p < 0.05$) oscillatory shear resulted in a statistically significant increase in cell invasion into the collagen I matrix, which is representative of an advanced stage of EndMT (Figure 3). We did not take into account the total number of cells per field, which is generally lower for oscillatory conditions. The lower cell density found in the oscillatory shear conditions would result in a higher fraction of invading cells, however. PAVEC exposed to steady shear are elongated in shape and have F-actin fibers aligned perpendicular to the shear flow direction (Figures 4A–C, 5 A–B). Oscillatory shear results in short, fragmented F-actin filaments, which did not allow for fiber alignment analysis (Figure 4 D–F). Cells exposed to oscillatory shear are also more circular when compared with those exposed to steady shear of the same magnitude (Figure 5A).

We next quantified changes in PAVEC EndMT-related protein and gene expression following static culture or exposure to 2, 10, or 20 dyne/cm^2 steady or oscillatory shear. Figure 6 is confocal images of endothelial (PECAM-1, red) and mesenchymal (αSMA, green) protein expression in the steady and oscillatory sheared cells and shows that αSMA expression increases and PECAM-1 expression decreases in laminar 2 dyne/cm^2 and oscillatory 2 and 10 dyne/cm^2 conditions. Figure 7 shows quantified αSMA protein expression. Cells exposed to static conditions, 10 dyne/cm^2, or 20 dyne/cm^2 steady shear showed significantly less αSMA expression when compared with 2 dyne/cm^2 steady shear (Figure 7A, $p < 0.05$), and cells exposed to ±2 dyne/cm^2 or ±10 dyne/cm^2 oscillatory shear showed significantly more αSMA protein expression when compared with static controls and cells exposed to ±20 dyne/cm^2 oscillatory shear (Figure 7B, $p < 0.05$). We found that PAVEC exposed to steady shear showed a general trend of decreasing mesenchymal protein markers with increasing steady shear stress rates when compared with static controls, while PAVEC exposed to oscillatory shear showed a general trend of increased mesenchymal protein markers when compared with static controls.

Finally, we measured PAVEC pro-EndMT (ACTA2, Snail, TGFB1) and inflammatory (VCAM1, ICAM1, NFKB1) gene expression in response to steady and oscillatory shear. Exposure to 2 dyne/cm^2 steady shear significantly upregulated pro-EndMT (ACTA2 6.0±2.0 fold increase over static control, $p < 0.05$; Snail 4.1±0.8 fold increase over static control, $p < 0.05$) and inflammatory (ICAM1, NFKB1) gene expression when compared with higher steady shear stresses and static controls (Figures 8A,B). High steady shear (20 dyne/cm^2)

significantly increased gene expression of PECAM1, an endothelial marker (15.9±6.6 fold increase over static control, $p < 0.05$). VCAM1 gene expression was significantly decreased for PAVEC exposed to all steady shear stresses when compared with static controls (Figure 8B). When compared to static controls and steady shear, oscillatory shear of all levels induced a significant upregulation in the EndMT-related and inflammatory genes ACTA2, Snail, TGFB1, ICAM1, and NFKB in PAVEC (Figures 8 C, D). These results indicate that oscillatory shear at low magnitudes (2 and 10 dyne/cm^2) and steady shear at low magnitude (2 dyne/cm^2) induce EndMT, while high magnitude steady shear (10 and 20 dyne/cm^2) is protective against this behavior. We have shown that inflammation promotes EndMT through a nuclear factor-κB–dependent pathway (Mahler et al. 2013). This work, as well as previous work (Sucosky et al. 2009), supports inflammation induction in valve endothelial cells by low steady shear and oscillatory shear, and our work shows that low steady shear and oscillatory shear also promote inflammatory EndMT.

Discussion

The valve structure is subdivided into three distinct layers: The fibrosa (located on the aortic side of the leaftet), ventricularis (located on the ventricular surface of the leaflet), and spongiosa (located between the fibroas and the ventricularis) (Christie 1992). In healthy valves, the fibrosa matrix is primarily composed of circumferentially-aligned, collagen I fibers(Vesely and Noseworthy 1992), while the ventricularis contains more elastin than the fibrosa(Vesely 1997). Studies measuring the stiffness of the aortic valve layers have shown that most of the valvular structural support is provided by the collagen-rich fibrosa layer(Sewell-Loftin et al. 2012; Zhao et al. 2011).We therefore chose to use 3D collgen I gels to mimic the aortic valve ECM. We chose to study valve endothelial cell behavior on 1.5 mg/mL collagen I gels. Our previous work has shown that a collagen concentration of more than 1.5 mg/mL provides a matrix that is too biomechanically stiff for the cells to move through, making invasion assays difficult (Mahler et al. 2010). Collagen gel concentrations lower than 1.5 mg/mL have so few collagen fibers that the cells can shred the fibers locally, producing an island of cells (Mahler et al. 2010). Future work may focus on changes to the biomechanics of the ECM and matrix protein composition, as both may be related to shear stress responsiveness(Orr et al. 2006).

Previous work has shown that oscillatory shear (±4 dyne/cm^2) on vascular endothelial cells resulted in a rounded cell shape with random and short actin filaments (Chiu et al. 1998). Steady shear stress (20 dyne/cm^2) on vascular and valvular endothelial cells results in an elongated cell shape, however, with vascular endothelial cell actin fibers aligning parallel to the shear flow direction and valvular endothelial cell F-actin aligning perpendicular to shear (Butcher et al. 2004; Chiu and Chien 2011). Our results agree with previous *in vitro* work, as steady shear on PAVEC resulted in elongated cells with F-actin aligned perpendicular to the shear flow direction, while oscillatory shear on PAVEC resulted in a rounded cells shape and short, randomly distributed F-actin filaments. Disturbed flow can cause pro-inflammatory cytokine release (BMP2/4) and a pro-oxidant phenotype, including producing reactive oxygen species (ROS) from reduced nicotinamide adenine dinucleotide phosphate (NADPH) oxidases in valve endothelial cells (Butcher et al. 2006; Sorescu et al. 2004; Sucosky et al. 2009). Low magnitude oscillatory shear (≤ ±5 dyne/cm^2) and low steady

shear stress has also been shown to promote an atherogentic phenotype and inflammatory activation in vascular endothelial cells (Brooks et al. 2002; Brooks et al. 2004; Chappell et al. 1998; Davies et al. 2001; De Keulenaer et al. 1998; Malek et al. 1999). This occurs in parallel with the loss of endothelial alignment and a larger and more rounded appearance, similar to endothelial cells in arterial bifurcations or endothelial cells exposed to reversed flow *in vivo* (Levesque et al. 1986; Sarphie 1985). Our previous work has also shown EndMT on the fibrosa side of adult valves, which is exposed to oscillatory shear and is the initiating site of inflammatory and calcific degeneration (Mohler 2000; Mohler 2004; Mohler et al. 2001); while on the ventricularis, which is exposed to high steady shear stress, EndMT is absent (Mahler et al. 2013). The results presented here are consistent with these *in vitro* and *in vivo* findings. Exposure to low steady shear stress and oscillatory shear stress resulted in an upregulation of inflammatory gene expression, EndMT-related gene and protein expression, and cell invasion; while high steady shear stress was protective against inflammation and EndMT. While previous work has shown an upregulation in the endothelial adhesion molecules ICAM-1 and VCAM-1 in response to altered shear stress profiles (Sucosky et al. 2009), our work is the first to determine the role of hemodynamics on adult EndMT and to show that low magnitude, but not high magnitude oscillatory shear stress, and low magnitude steady shear stress cause inflammatory conditions and EndMT. We recognize that not all shear stress conditions studies represent naturally occurring shear stress in the aortic valve (i.e. 2 dyne/cm^2 steady shear stress and 20 dyne/cm^2 oscillatory shear stress), but these conditions are nonetheless important to include for a fundamental understanding and mechanism of shear-induced adult EndMT.

Studying cell behavior, including EndMT, under physiological conditions is critical, but the complexity of the *in vivo* environment makes identifying the specific effects of mechanical stimuli challenging. *In vitro* experiments provide a platform for determining the influence of individual mechanical forces on cell function, but the mechanical stimulation of cell cultures in macroscale devices is often tightly coupled to other stimulation modes (i.e. solid deformation, fluid flows, altered physical and chemical surface features, and a complex transfer of loads between the various interacting components) (Moraes et al. 2011). This makes connecting a biological response with a specific mechanical stimulus problematic. Microfluidic devices can generate insight into the mechanical nature of cell behavior by decoupling stimulation parameters, enabling multimodal control over combinations of stimuli, and increasing experimental throughput (Moraes et al. 2011). Our device design allows for study of cell behavior in response to multiple shear stress rates, in 3D culture conditions, in real time, and provides a simplified method for the addition of 3D culture matrix and cell seeding.

Conclusions

We have developed and implemented a shear stress bioreactor that is broadly useful for exposing endothelial cells seeded on a physiologically realistic 3D matrix to varying steady or oscillatory shear stresses. The flow profile within the bioreactor was characterized both computationally and experimentally and shown to accurately mimic calculated shear stress values. Endothelial cell invasion, alignment, and EndMT-related gene and protein expression was evaluated following exposure to varying rates of steady and oscillatory

shear. For the adult cells we found that low steady shear stress (2 dyne/cm^2) and oscillatory shear stress upregulated EndMT and inflammation-related gene and protein expression when compared with static controls or cells exposed to high steady shear (10 and 20 dyne/cm^2). EndMT is an important valve morphogenic mechanism, and our previous work has shown that mesenchymal transformation may also play a role in adult valve disease (Mahler et al. 2013). Understanding the role of hemodynamics on EndMT is critical as the re-emergence of embryonic phenotypes of valvular endothelial cells may be an important mechanism of valvular disease initiation and/or progression.

Supplementary Material

Refer to Web version on PubMed Central for supplementary material.

Acknowledgements

This work was supported by The Hartwell Foundation (JTB), The Hartwell Foundation Postdoctoral Fellowship (GJM), the National Institute of Health (HL110328 JTB, 1R15ES022828 GJM), the National Science Foundation (CBET-0955712 JTB), the American Heart Association Scientist Development Grant (#0830384N, JTB), the LeDucq Foundation (Project MITRAL, JTB) and the Michael Connolly Endowment Fund (GJM).

References

Balachandran K, Alford PW, Wylie-Sears J, Goss JA, Grosberg A, Bischoff J, Aikawa E, Levine RA, Parker KK. Cyclic strain induces dual-mode endothelial-mesenchymal transformation of the cardiac valve. Proc Natl Acad Sci U S A. 2011; 108(50):19943–19948. [PubMed: 22123981]

Brooks AR, Lelkes PI, Rubanyi GM. Gene expression profiling of human aortic endothelial cells exposed to disturbed flow and steady laminar flow. Physiol Genomics. 2002; 9(1):27–41. [PubMed: 11948288]

Brooks AR, Lelkes PI, Rubanyi GM. Gene Expression Profiling of Vascular Endothelial Cells Exposed to Fluid Mechanical Forces: Relevance for Focal Susceptibility to Atherosclerosis. Endothelium. 2004; 11(1):45–57. [PubMed: 15203878]

Butcher JT, Mahler GJ, Hockaday LA. Aortic valve disease and treatment: The need for naturally engineered solutions. Adv Drug Deliver Rev. 2011; 63(4–5):242–268.

Butcher JT, Nerem RM. Valvular endothelial cells regulate the phenotype of interstitial cells in co-culture: effects of steady shear stress. Tissue Eng. 2006; 12(4):905–915. [PubMed: 16674302]

Butcher JT, Nerem RM. Valvular endothelial cells and the mechanoregulation of valvular pathology. Philos Trans R Soc Lond B Biol Sci. 2007; 362(1484):1445–1457. [PubMed: 17569641]

Butcher JT, Penrod AM, Garcia AJ, Nerem RM. Unique morphology and focal adhesion development of valvular endothelial cells in static and fluid flow environments. Arterioscler Thromb Vasc Biol. 2004; 24(8):1429–1434. [PubMed: 15117733]

Butcher JT, Tressel S, Johnson T, Turner D, Sorescu G, Jo H, Nerem RM. Transcriptional profiles of valvular and vascular endothelial cells reveal phenotypic differences: Influence of shear stress. Arterioscler Thromb Vasc Biol. 2006; 26(1):69–77. [PubMed: 16293796]

Chappell DC, Varner SE, Nerem RM, Medford RM, Alexander RW. Oscillatory Shear Stress Stimulates Adhesion Molecule Expression in Cultured Human Endothelium. Circulation Research. 1998; 82(5):532–539. [PubMed: 9529157]

Chen H, Cornwell J, Zhang H, Lim T, Resurreccion R, Port T, Rosengarten G, Nordon RE. Cardiac-like flow generator for long-term imaging of endothelial cell responses to circulatory pulsatile flow at microscale. Lab on a Chip. 2013a; 13(15):2999–3007. [PubMed: 23727941]

Chen MB, Srigunapalan S, Wheeler AR, Simmons CA. A 3D microfluidic platform incorporating methacrylated gelatin hydrogels to study physiological cardiovascular cell-cell interactions. Lab on a Chip. 2013b; 13(13):2591–2598. [PubMed: 23525275]

Chiu J-J, Chien S. Effects of Disturbed Flow on Vascular Endothelium: Pathophysiological Basis and Clinical Perspectives. Physiological Reviews. 2011; 91(1):327–387. [PubMed: 21248169]

Chiu JJ, Wang DL, Chien S, Skalak R, Usami S. Effects of disturbed flow on endothelial cells. J Biomech Eng. 1998; 120(1):2–8. [PubMed: 9675673]

Christie GW. Anatomy of aortic heart valve leaflets: the influence of glutaraldehyde fixation on function. Eur J Cardiothorac Surg. 1992; 6(suppl_1):S25–S33. [PubMed: 1389275]

Davies PF, Shi C, DePaola N, Helmke BP, Polacek DC. Hemodynamics and the Focal Origin of Atherosclerosis. Annals of the New York Academy of Sciences. 2001; 947(1):7–17. [PubMed: 11795312]

De Keulenaer GW, Chappell DC, Ishizaka N, Nerem RM, Alexander RW, Griendling KK. Oscillatory and Steady Laminar Shear Stress Differentially Affect Human Endothelial Redox State : Role of a Superoxide-Producing NADH Oxidase. Circulation Research. 1998; 82(10):1094–1101. [PubMed: 9622162]

Egorova AD, Khedoe PPSJ, Goumans M-JTH, Yoder BK, Nauli SM, ten Dijke P, Poelmann RE, Hierck BP. Lack of Primary Cilia Primes Shear-Induced Endothelial-to-Mesenchymal Transition. Circ Res. 2011; 108(9):1093–1101. [PubMed: 21393577]

Gould RA, Butcher JT. Isolation of valvular endothelial cells. J Vis Exp. 2010; 46(e2158)

Hsu Y-H, Moya ML, Abiri P, Hughes CCW, George SC, Lee AP. Full range physiological mass transport control in 3D tissue cultures. Lab on a Chip. 2013; 13(1):81–89. [PubMed: 23090158]

Kilner PJ, Yang G-Z, Wilkes AJ, Mohiaddin RH, Firmin DN, Yacoub MH. Asymmetric redirection of flow through the heart. Nature. 2000; 404(6779):759–761. [PubMed: 10783888]

Levesque MJ, Liepsch D, Moravec S, Nerem RM. Correlation of endothelial cell shape and wall shear stress in a stenosed dog aorta. Arteriosclerosis, Thrombosis, and Vascular Biology. 1986; 6(2): 220–229.

Lu H, Koo LY, Wang WM, Lauffenburger DA, Griffith LG, Jensen KF. Microfluidic Shear Devices for Quantitative Analysis of Cell Adhesion. Analytical Chemistry. 2004; 76(18):5257–5264. [PubMed: 15362881]

Mahler GJ, Farrar EJ, Butcher JT. Inflammatory cytokines promote mesenchymal transformation in embryonic and adult valve endothelial cells. Arteriosclerosis, Thrombosis, and Vascular Biology. 2013; 33:121–130.

Mahler GJ, Gould RA, Butcher JT. Isolation and culture of avian embryonic valvular progenitor cells. J Vis Exp. 2010; 44(e2159)

Malek AM, Alper SL, Izumo S. Hemodynamic shear stress and its role in atherosclerosis. JAMA. 1999; 282(21):2035–2042. [PubMed: 10591386]

Markwald RR, Fitzharris TP, Manasek FJ. Structural development of endocardial cushions. Am J Anat. 1977; 148(1):85–119. [PubMed: 842477]

Markwald RR, Fitzharris TP, Smith WN. Sturctural analysis of endocardial cytodifferentiation. Dev Biol. 1975; 42(1):160–180. [PubMed: 1112439]

Mohler ER 3rd. Are atherosclerotic processes involved in aortic-valve calcification? Lancet. 2000; 356(9229):524–525. [PubMed: 10950224]

Mohler ER 3rd. Mechanisms of aortic valve calcification. Am J Cardiol. 2004; 94(11):1396–1402. A6. [PubMed: 15566910]

Mohler ER III, Gannon F, Reynolds C, Zimmerman R, Keane MG, Kaplan FS. Bone formation and inflammation in cardiac valves. Circulation. 2001; 103(11):1522–1528. [PubMed: 11257079]

Moraes C, Sun Y, Simmons CA. (Micro)managing the mechanical microenvironment. Integrative Biology. 2011; 3(10):959–971. [PubMed: 21931883]

Nakajima Y, Mironov V, Yamagishi T, Nakamura H, Markwald RR. Expression of smooth muscle alpha-actin in mesenchymal cells during formation of avian endocardial cushion tissue: A role for transforming growth factor b3. Dev Dynam. 1997; 209(3):296–309.

Nandy S, Tarbell JM. Flush mounted hot film anemometer measurement of wall shear stress distal to a tri-leaflet valve for Newtonian and non-Newtonian blood analog fluids. Biorheology. 1987; 24(5): 483–500. [PubMed: 2965604]

Orr AW, Ginsberg MH, Shattil SJ, Deckmyn H, Schwartz MA. Matrix-specific Suppression of Integrin Activation in Shear Stress Signaling. Molecular Biology of the Cell. 2006; 17(11):4686–4697. [PubMed: 16928957]

Paranya G, Vineberg S, Dvorin E, Kaushal S, Roth SJ, Rabkin E, Schoen FJ, Bischoff J. Aortic valve endothelial cells undergo transforming growth factor-b-mediated and non-transforming growth factor-b-mediated transdifferentiation in vitro. Am J Pathol. 2001; 159(4):1335–1343. [PubMed: 11583961]

Poggianti E, Venneri L, Chubuchny V, Jambrik Z, Baroncini LA, Picano E. Aortic valve sclerosis is associatedwith systemic endothelial dysfunction. Journal of the American College of Cardiology. 2003; 41(1):136–141. [PubMed: 12570956]

Sarphie TG. Surface responses of aortic valve endothelia from diet-induced, hypercholesterolemic rabbits. Atherosclerosis. 1985; 54(3):283–299. [PubMed: 3994784]

Schneider CA, Rasband WS, Eliceiri KW. NIH Image to ImageJ: 25 years of image analysis. Nat Methods. 2012; 9(7):671–675. [PubMed: 22930834]

Schneider PJ, Deck JD. Tissue and cell renewal in the natural aortic valve of rats: an autoradiographic study. Cardiovascular Research. 1981; 15(4):181–189. [PubMed: 7273050]

Sewell-Loftin MK, Brown CB, Baldwin HS, Merryman WD. A novel technique for quantifying mouse heart valve leaflet stiffness with atomic force microscopy. J Heart Valve Dis. 2012; 21(4):513–520. [PubMed: 22953681]

Shao J, Wu L, Wu J, Zheng Y, Zhao H, Jin Q, Zhao J. Integrated microfluidic chip for endothelial cells culture and analysis exposed to a pulsatile and oscillatory shear stress. Lab on a Chip. 2009; 9(21): 3118–3125. [PubMed: 19823728]

Sorescu GP, Song H, Tressel SL, Hwang J, Dikalov S, Smith DA, Boyd NL, Platt MO, Lassegue B, Griendling KK, et al. Bone morphogenic protein 4 produced in endothelial cells by oscillatory shear stress induces monocyte adhesion by stimulating reactive oxygen species production from a Nox1-based NADPH oxidase. Circ Res. 2004; 95(8):773–779. [PubMed: 15388638]

Sucosky P, Balachandran K, Elhammali A, Jo H, Yoganathan AP. Altered shear stress stimulates upregulation of endothelial VCAM-1 and ICAM-1 in a BMP-4 and TGF-b1-dependent pathway. Arterioscler Thromb Vasc Biol. 2009; 29(2):254–260. [PubMed: 19023092]

Sun HB, Yokota H. Messenger-RNA expression of matrix metalloproteinases, tissue inhibitors of metalloproteinases, and transcription factors in rheumatic synovial cells under mechanical stimuli. Bone. 2001; 28(3):303–309. [PubMed: 11248661]

ten Dijke P, Egorova AD, Goumans M-JTH, Poelmann RE, Hierck BP. TGF-{beta} Signaling in Endothelial-to-Mesenchymal Transition: The Role of Shear Stress and Primary Cilia. Sci. Signal. 2012; 5(212) pt2-.

Thubrikar M, Klemchuk PP, Thubrikar M. The aortic valve: CRC press Florida eBoca Raton Boca Raton. 1990

Vesely I. The role of elastin in aortic valve mechanics. J Biomech. 1997; 31(2):115–123. [PubMed: 9593204]

Vesely I, Noseworthy R. Micromechanics of the fibrosa and the ventricularis in aortic valve leaflets. J Biomech. 1992; 25(1):101–113. [PubMed: 1733978]

Vickerman V, Blundo J, Chung S, Kamm R. Design, fabrication and implementation of a novel multi-parameter control microfluidic platform for three-dimensional cell culture and real-time imaging. Lab on a Chip. 2008; 8(9):1468–1477. [PubMed: 18818801]

Weston MW, LaBorde DV, Yoganathan AP. Estimation of the shear stress on the surface of an aortic valve leaflet. Annals of Biomedical Engineering. 1999; 27(4):572–579. [PubMed: 10468241]

Yap C, Saikrishnan N, Tamilselvan G, Yoganathan A. Experimental measurement of dynamic fluid shear stress on the aortic surface of the aortic valve leaflet. Biomechanics and Modeling in Mechanobiology. 2012a; 11(1–2):171–182. [PubMed: 21416247]

Yap C, Saikrishnan N, Yoganathan A. Experimental measurement of dynamic fluid shear stress on the ventricular surface of the aortic valve leaflet. Biomechanics and Modeling in Mechanobiology. 2012b; 11(1–2):231–244. [PubMed: 21465260]

Zhao R, Sider KL, Simmons CA. Measurement of layer-specific mechanical properties in multilayered biomaterials by micropipette aspiration. Acta Biomaterialia. 2011; 7(3):1220–1227. [PubMed: 21056128]

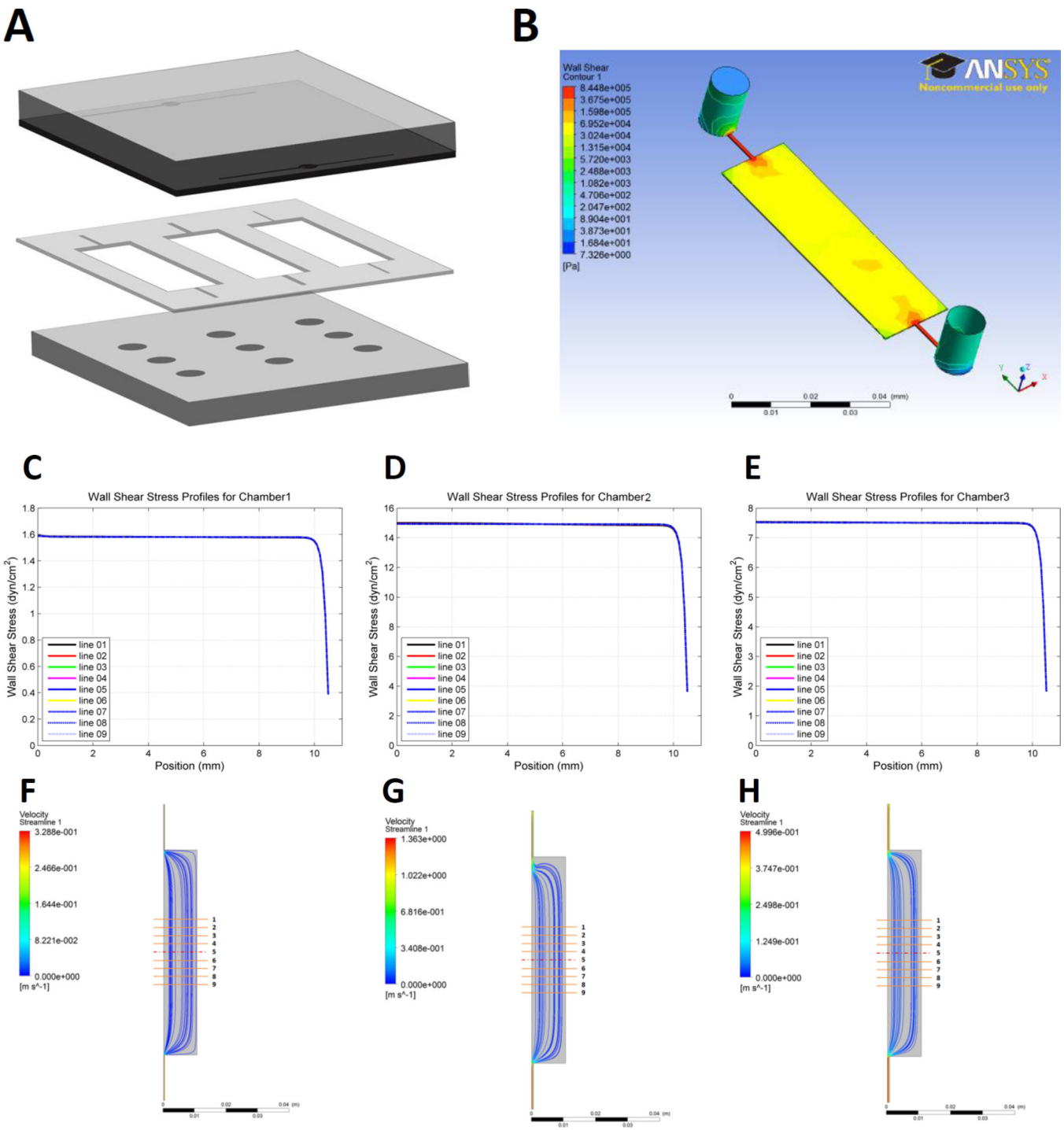

Fig. 1.

(A) Schematic of the shear stress bioreactor. (B) The bioreactor set-up for steady shear experiments, (C) the 3D parallel plate bioreactor, and (D) the bioreactor arranged with a syringe pump for oscillatory shear experiments.

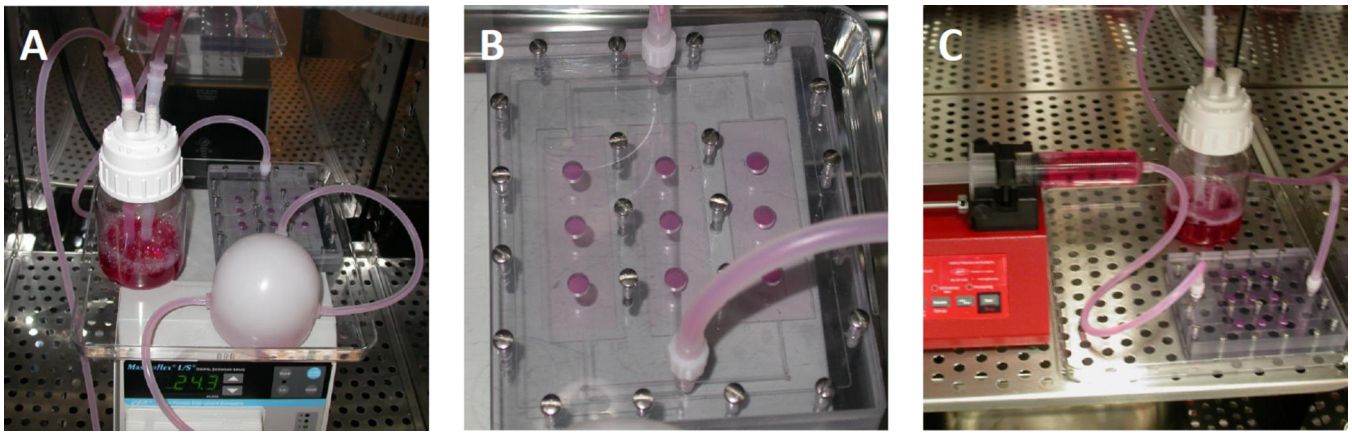

Fig. 2.

Simulated flow streamlines for the 2 (A), 10 (B), and 20 (C) dyne/cm^2 chambers under steady shear conditions with a graph of corresponding simulated wall shear stress values at nine different sites. Dotted lines represent approximate gel location.

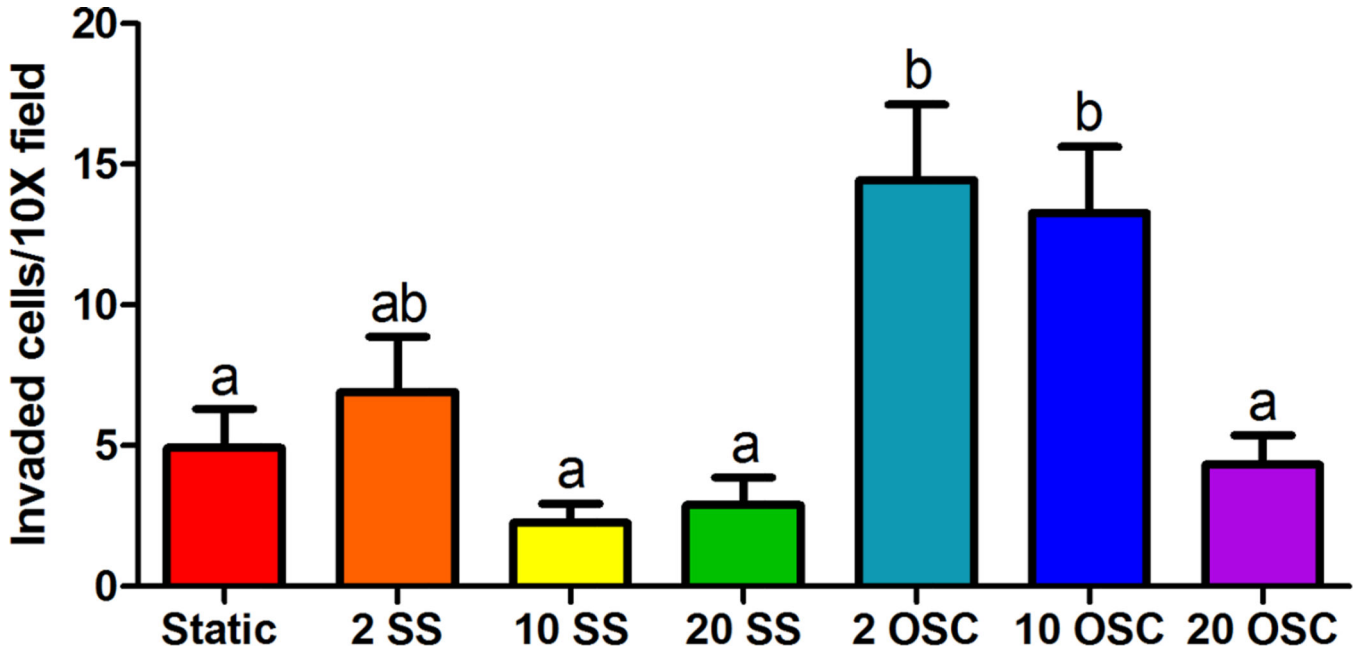

Fig. 3.

Porcine aortic valve endothelial cell (PAVEC) invasion into the collagen matrix after a 48 hour exposure to 2, 10, or 20 dyne/cm^2 steady or oscillatory shear. Error bars show ±SEM, n = 6. Bars that do not share any letters are significantly different according to a one-way ANOVA with Tukey's post-test ($p \leq 0.05$).

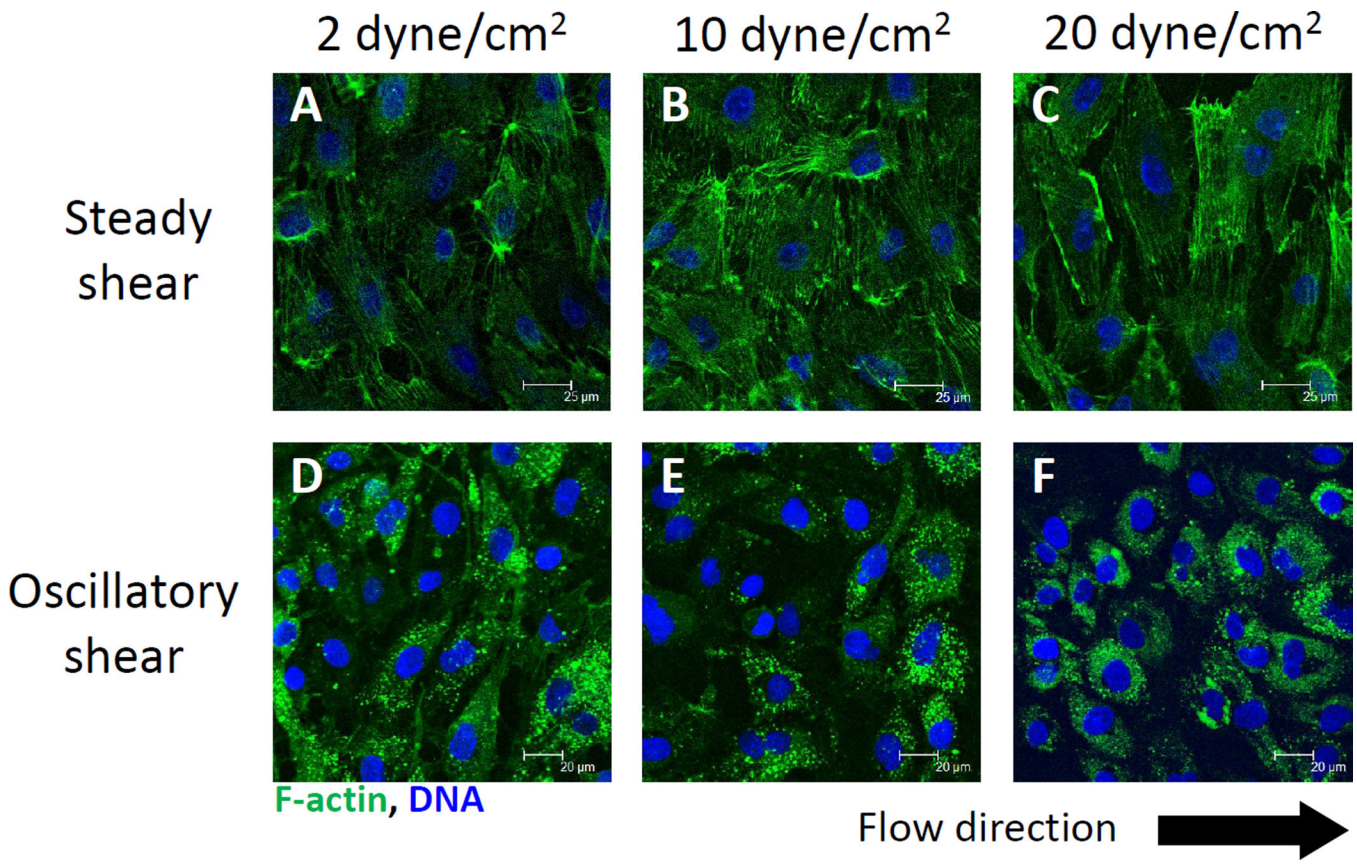

Fig. 4.

Porcine aortic valve endothelial cells (PAVEC) following 48 hours of exposure to 2 (A), 10 (B), or 20 (C) dyne/cm^2 steady or 2 (D), 10 (E), or 20 (F) dyne/cm^2 oscillatory shear. Cells are stained for F-actin (green) and DNA (blue), and arrows indicate the fluid flow direction.

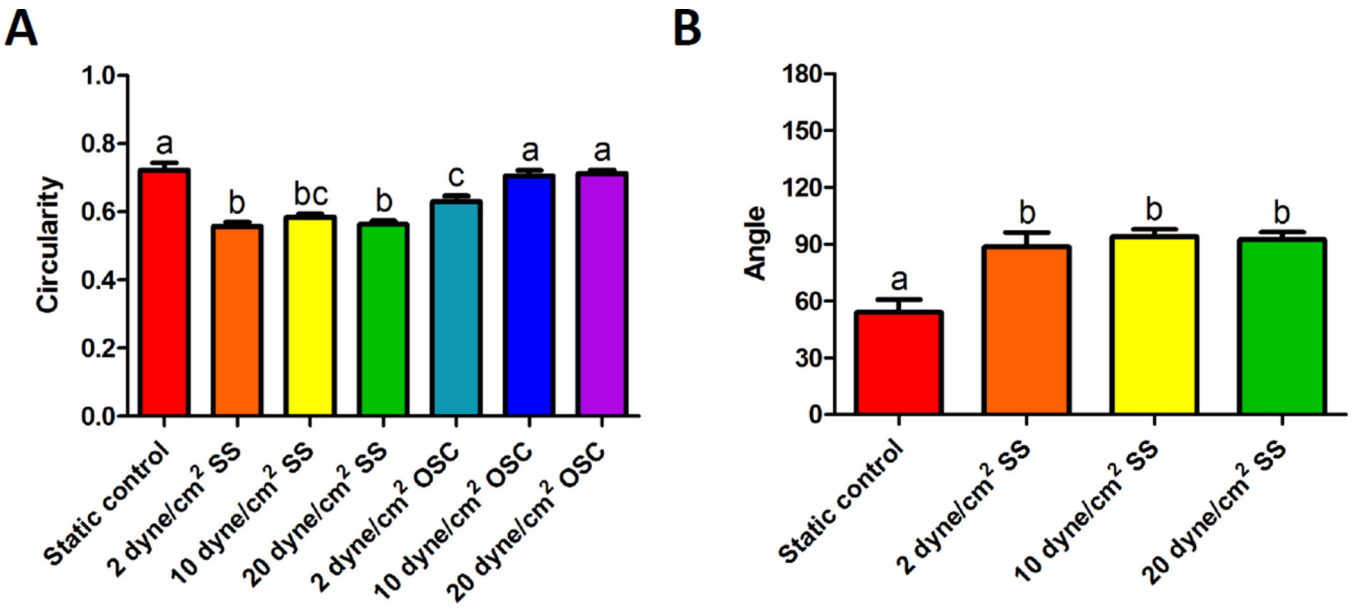

Fig. 5.

Image analysis of cells following 48 hours steady (SS) or oscillatory (OSC) shear exposure. (A) Cell circularity, (B) F-actin alignment for steady shear. Error bars show ±SEM, n = at least 50 cells from 10 representative confocal images. Bars that do not share any letters are significantly different according to a one-way ANOVA with Tukey's post-test ($p \leq 0.05$).

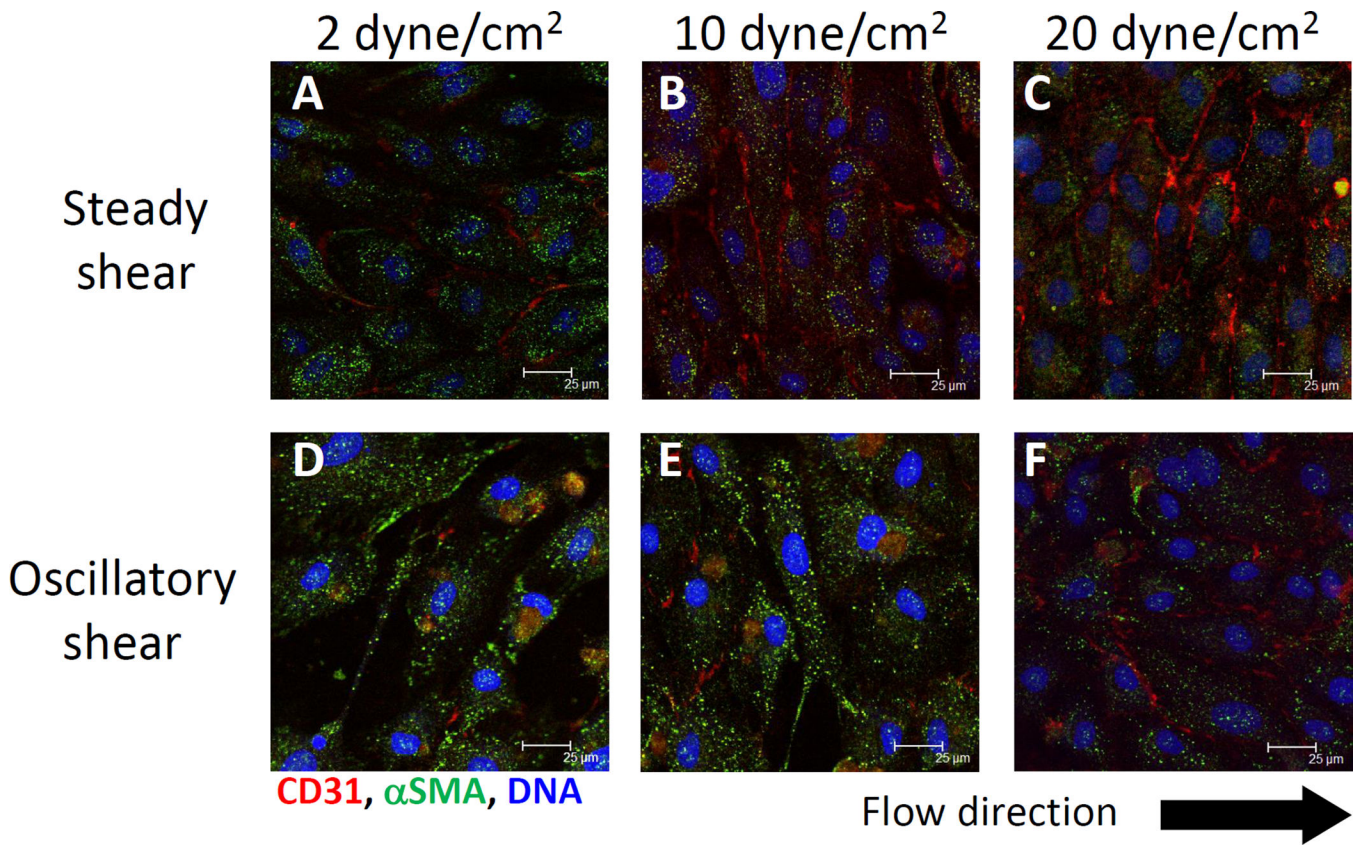

Fig 6.

Porcine aortic valve endothelial cells (PAVEC) following 48 hours of exposure to 2 (A), 10 (B), or 20 (C) dyne/cm^2 steady or 2 (D), 10 (E), or 20 (F) dyne/cm^2 oscillatory shear. Panel G shows porcine aortic valve interstitial cells seeded onto a 3D collagen I gel and grown for 48 hours in static conditions, and panel H is PAVEC seeded onto a 3D collagen I gel and grown for 48 hours in static conditions. Cells are stained for PECAM-1 (red), αSMA (green), and DNA (blue), arrows indicate the fluid flow direction.

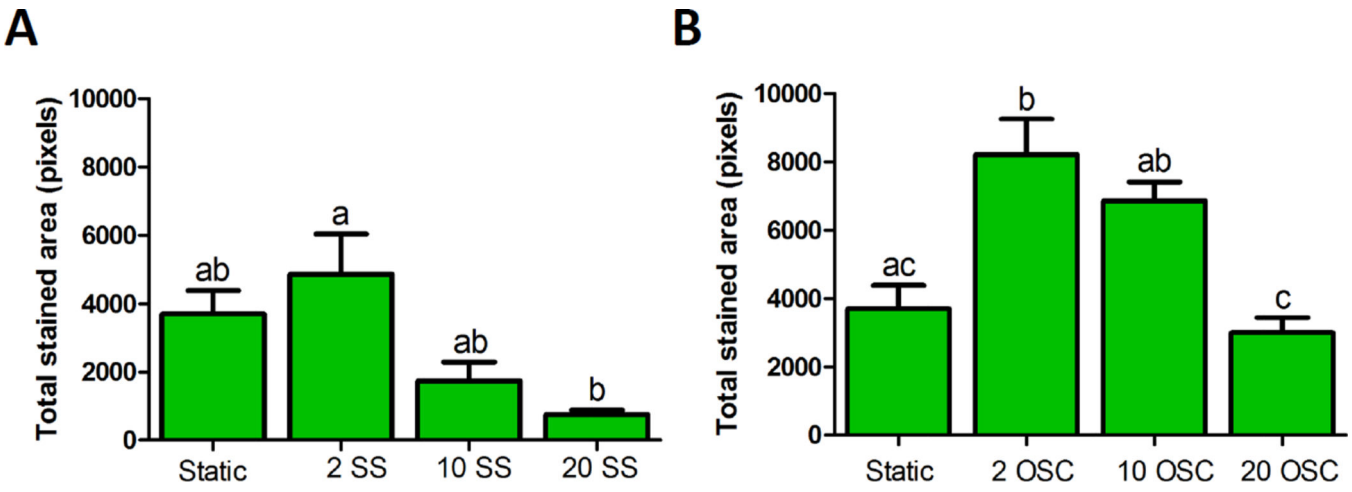

Fig. 7.

Protein quantification of cells following 48 hours steady (SS) or oscillatory (OSC) shear exposure. (A) αSMA expression per cell in steady sheared cells, and (B) αSMA per cell expression in oscillatory sheared cells. Error bars show ±SEM, n = at least 50 cells from 10 representative confocal images. Bars that do not share any letters are significantly different according to a one-way ANOVA with Tukey's post-test ($p \leq 0.05$).

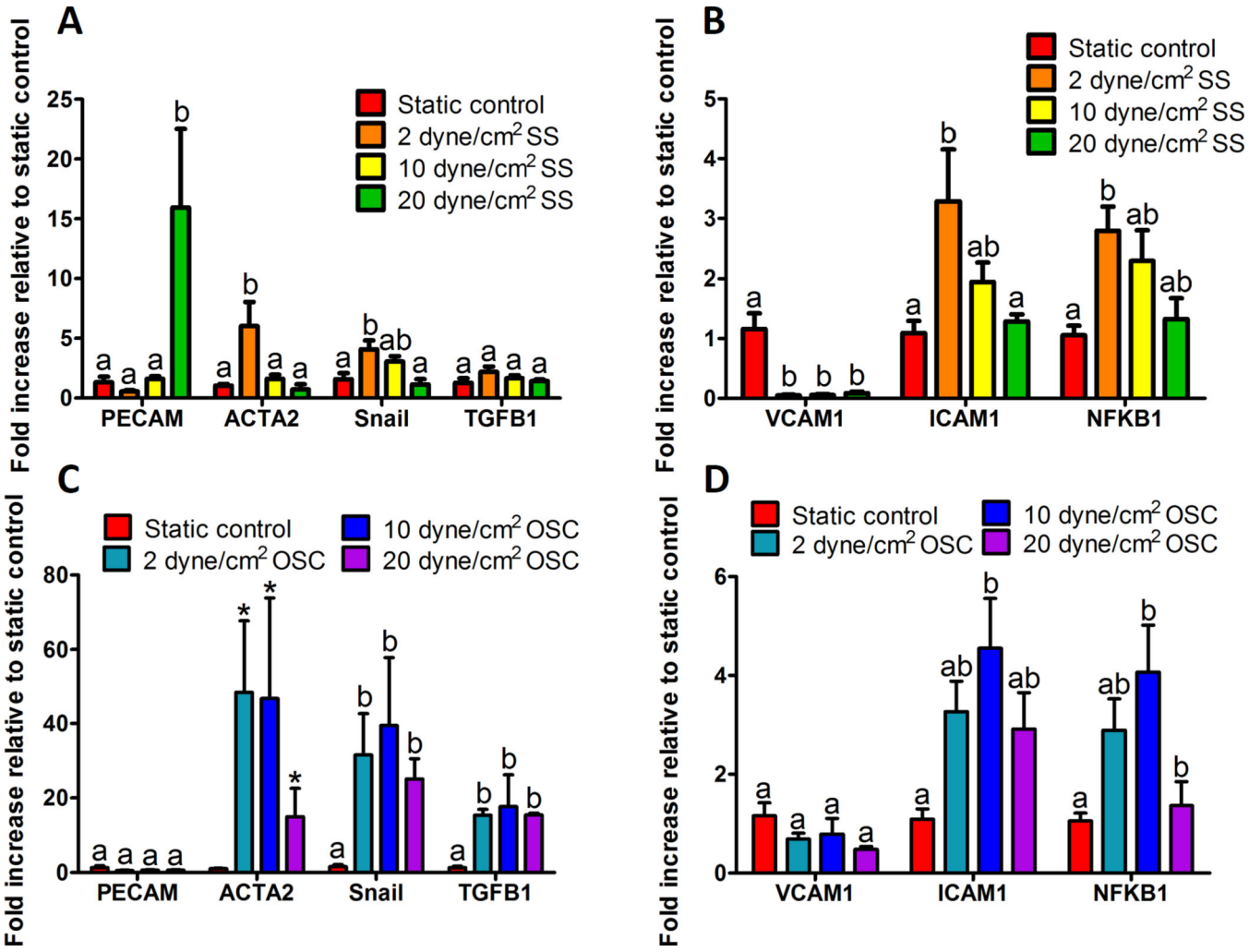

Fig. 8.

Porcine aortic valve endothelial cells (PAVEC) EndMT-related (A, C) and inflammatory (B, D) gene expression following 48 hours of exposure to steady (A, B; SS) or oscillatory (C, D; OSC) shear stress. Error bars show ±SEM, n = 6. Bars that do not share any letters are significantly different according to a one-way ANOVA with Tukey's post-test ($p \leq 0.05$).

Table I

Comparison between calculated and experimentally measured residence times and linear velocities. Values are expressed as mean ±SEM, n = 3 for residence time measurements, n = 25 particles for linear velocity measurements.

	Low Steady Shear (1 dyne/cm^2)	**Mid Steady Shear (5 dyne/cm^2)**	**High Steady Shear (10 dyne/cm^2)**
Residence time (calculated, s)	40.56	8.52	4.26
Residence time (measured, s)	39.53 ± 1.78	8.60 ± 0.21	4.87 ± 0.23